

Impact of copper inserts in collector bars

René von Kaenel, Jacques Antille, Louis Bugnion
KAN-NAK Ltd., Route de Sion 35, 3960 Sierre, Switzerland

Keywords: Copper insert, Energy saving, Magneto-hydrodynamic, Cell design, Current efficiency, Velocity field, Metal deformation

Abstract

The use of copper inserts in collector bars has been tested in the booster section of one line. The impact on the metal velocity field, metal deformation, cell magneto-hydrodynamic state and operational data has been computed for a Reference cell and for the “Copper insert” cell. In-situ measurements in the collector bars and numerous other measurements were performed to evaluate the impact after 6 months operation. The model and measurements show a very good agreement and the results are very promising.

Introduction

Cathode design remains an interesting field of investigation to achieve lower specific energy consumption, longer cell life and improved current efficiency. The current density field in the liquid metal is strongly dependent on the cathode design. A number of cathode shapes have been presented for many years as shown in Figure 1.

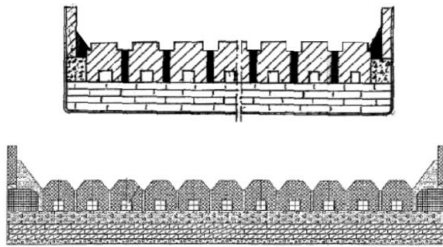


Figure 1: Shaped cathode surface “Vittorio de Nora” 1994

Novel Structural Cathodes (NSC) have been tested in China. The cathode design involves the shape, the physical properties and most important the collector bars leading the current outside the cell. A number of recent solutions are discussed in References [1-9]. The use of copper inserts is highlighted in Reference [3]. This paper presents the impact of using copper inserts for one specific technology using standard flat cathode blocks. The thermal-electric and magneto-hydrodynamic effects are analyzed using MONA, a sophisticated 3D software for the modeling of the Hall-Héroult cells. The stationary state and the cell magneto-hydrodynamic stability are determined for a Reference cell without copper bars and for a modified lining using copper inserts in the collector bars. Modeling results are compared. The concept has been implemented in cells in a booster section to evaluate the potential. In-situ measurements have been performed in two collector bars to verify the impact of the copper inside the bars themselves. The voltage breakdown and key operational parameters have been measured. Figure 2 shows the collector bar with the cast iron for the Reference cell.

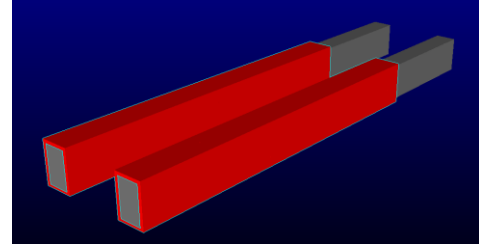


Fig 2: Collector bars with standard cast iron (Reference)

Figure 3 shows the bars with the copper inserts. The bar is also electrically insulated from the carbon cathode to improve the current density field inside the liquid metal. The key factors resides in the determination of the amount of copper to use, the length and position of the inserts, the length and position of the electrical insulation together with the bars cross section to achieve a low cathode voltage drop (CVD), the right heat extraction through the collector bars and the optimum current density field inside the liquid metal. Indeed, the current density inside the liquid metal interacts with the magnetic field which is generated by the current density itself and by the external busbars. Therefore, each technology is different, as the interaction depends on the busbars, anode positions, cathode grade, cathode shape, ledge profile and the copper must be optimized to these constraints.

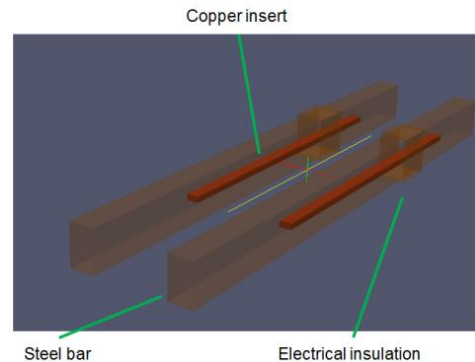


Fig 3: Copper insert inside collector bar

TE-Magneto-Hydrodynamic modeling of the Reference cell

The Reference cell was operated with the following parameters (Table 1).

Table 1: Key parameters of Reference cell

		Reference
Cell voltage	V	4.36
Current efficiency	%	93.8
Anode current density	A/cm ²	0.82
CVD	mV	281±20

The parameters are imposed to the model by boundary conditions

(current), heat balance equation (current efficiency), geometry (average metal height, average bath height) and material properties (solidus temperature, bath electrical conductivity). The full 3D cell geometry and every material component are also imbedded in the model. Each cell is made of more than 9 million elements. Neighboring cells are modeled in full 3D whereas cells at a larger distance are modeled as 3D wires. Material properties are all temperature dependent. The cell voltage is achieved by changing the ACD in the model. All other parameters are resulting from the calculations such as bath temperature, cell heat loss, external voltage, cathode voltage, etc...

Following parameters are calculated:

1. Thermal field in the cell and busbars
2. Ledge profile in the cell
3. Electric potential in the cell and busbars
4. Current density in the cell and busbars
5. Magnetic field inside the liquid metal and bath (ferromagnetic effects and induced currents are considered)
6. Velocity field of the liquid metal and bath (free interface bath-metal)
7. Metal surface contour (metal upheaval or interface bath-metal)
8. Anode current distribution when all anodes have the same ACD (the mean anode to cathode distance is automatically adjusted to obtain the total cell voltage, the shape of each anode is following the metal surface)
9. Collector bar current distribution
10. Partial voltage drops including CVD
11. Heat losses
12. Specific energy consumption
13. Cell MHD stability criteria

Figure 4 shows the electrical potential for the cathode. The CVD (average voltage from center of the liquid metal to collector bars ends) is calculated to be 291 mV. One can observe that the end blocks are showing some variation in the electrical potential due to the ledge (ridge) covering the cathode.

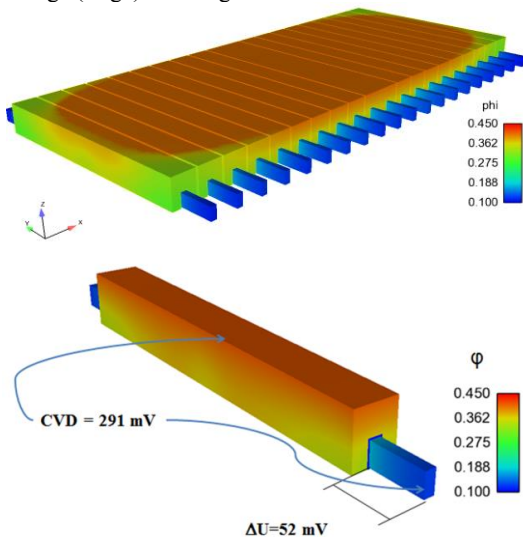


Fig 4: Calculated CVD for the Reference cell

Figure 5 shows the current density at the cathode surface for the Reference cell. A W shape can clearly be observed as a result of the cathode and collector bar designs.

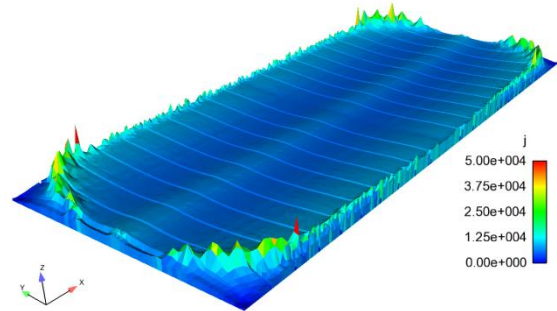


Fig 5: Current density at the surface of the cathode blocks, Reference cell

Figure 6 shows the current density profile for the center block. The current density is steadily growing from center to edge of the cathode block reaching more than 1.5 A/cm² at the edge. The slight decrease in the middle is due to horizontal current in the liquid metal as the current is looking for the minimum energy path.

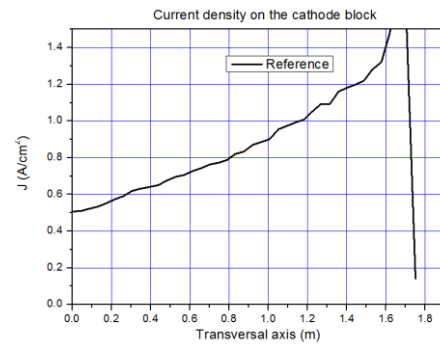
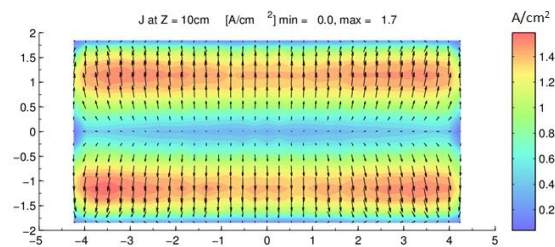


Fig 6: Current density profile at cathode surface, Reference cell

Figure 7 shows the current density inside the liquid metal. Strong horizontal components can be observed.

■ Current density inside the liquid metal (10 cm above the cathode)



$$|\vec{j}| = (j_x^2 + j_y^2 + j_z^2)^{1/2}$$

Figure 7: Horizontal current density inside liquid metal, Reference cell

Figure 8 shows the metal deformation. A metal upheaval of 8.6 cm over the whole metal surface is calculated.

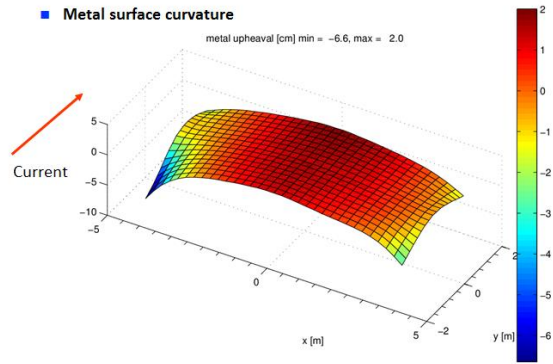


Figure 8: Metal deformation, Reference cell

Figure 9 shows the projection of the metal velocity field of the Reference cell in a plane located 10 cm above the carbon cathode level. The maximum speed in the plane is 13.5 cm/s, it is 25 cm/s when looking at the 3D maximum speed. The average velocity calculated from the average kinetic energy is 6.2 cm/s.

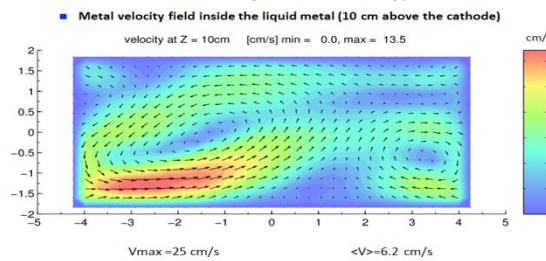


Fig 9: Metal velocity field, Reference cell

Last and most important of all figures is the cell stability diagram (Figure 10). The cell stability diagram shows the potential waves frequencies on the horizontal axis and the damping factor on the vertical axis (this value is directly correlated to the cell voltage noise factor). The low values are the destabilizing factors.

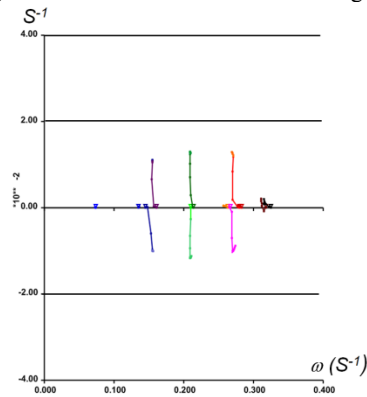


Fig 10: Cell stability diagram, Reference cell

TE-Magneto-Hydrodynamic modeling of the “Copper insert” cell

The lining was modified by implementing copper inserts and the thermal insulation was improved to be able to recover the potential energy saving. The basic calculated parameters are shown in Table 2.

Table 2: Key parameters of “Copper insert” cell

		“Copper insert”
Cell voltage	V	4.06
Current efficiency	%	95.0
Anode current density	A/cm ²	0.86
CVD	mV	260

Figure 11 shows the electrical potential for the cathode. The CVD (average voltage from center of the liquid metal to collector bars ends) is calculated to be 260 mV. One can observe that the end blocks show a much better potential distribution as the ledge shape was improved.

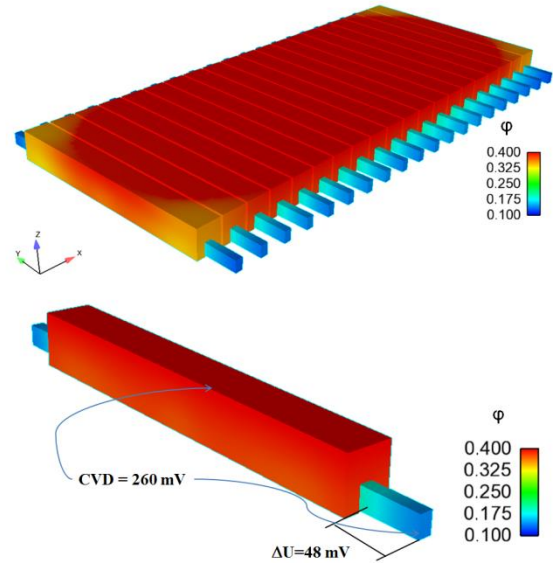


Fig 11: Calculated CVD for the “Copper insert” cell

Figure 12 shows the current density at the surface of the cathode for the “Copper insert” cell. The density is now always under 1 A/cm² in much better relation with the anode current density.

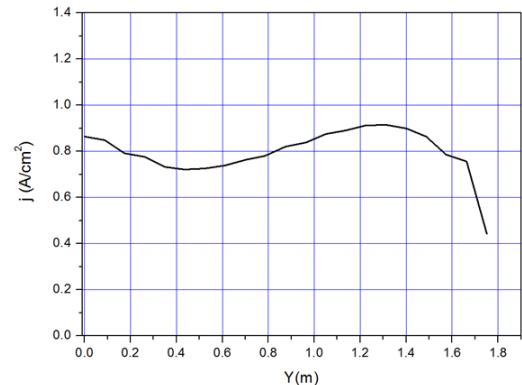


Fig 12: Current density profile at cathode surface, “Copper insert” cell

Figure 13 shows the current density inside the liquid metal. The strong horizontal components have fully disappeared.

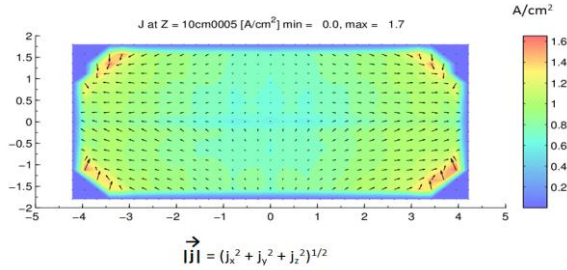


Fig 13: Horizontal current density inside liquid metal, "Copper insert" cell

Figure 14 shows the metal deformation. The metal upheaval has decreased by a factor three from 8.6 cm to 3.1 cm.

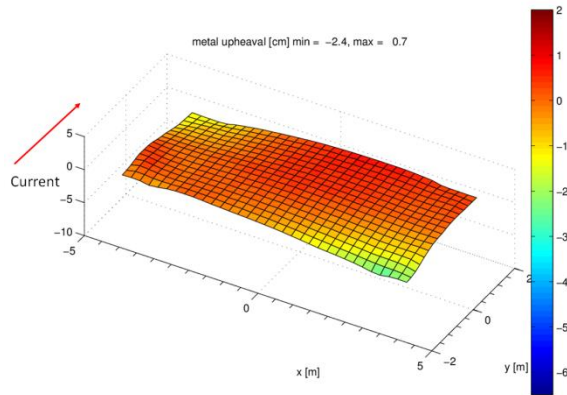


Fig 14: Metal deformation, "Copper insert" cell

Figure 15 shows the projection of the metal velocity field of the "Copper insert" cell in a plane located 10 cm above the carbon cathode level. The 3D maximum speed has decreased by a factor four from 25 cm/s to 6 cm/s. The average velocity calculated from the average kinetic energy is only 1.5 cm/s while the maximum velocity in the plane is 4.2 cm/s.

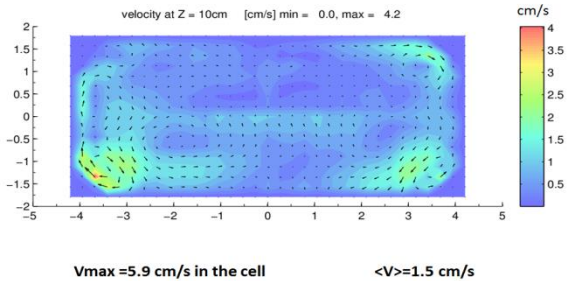


Fig 15: Metal velocity field, "Copper insert" cell

The cell stability diagram (Figure 16) only shows one potential destabilizing frequency and the damping factor is much more favorable.

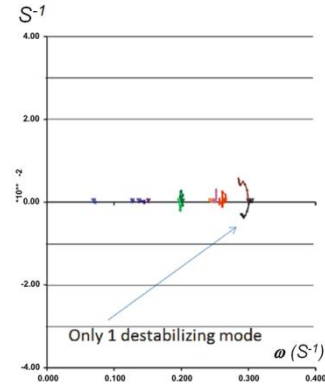


Fig 16: Cell stability diagram, "Copper insert" cell

The cell model was used to increase the current while decreasing the ACD in such a way that the internal heat production between the anodes and the collector bars ends would remain constant. By doing so, it was predicted that the "Copper insert" cell would yield the same level of stability as the Reference cells while increasing the current by 24% with a specific energy of 12.8 kWh/kg, assuming a constant current efficiency of 94%. In fact, due to the very low metal deformation, low velocity field and very good cell MHD stability, it was expected to improve the current efficiency at the same time. Let us see what the measurements have shown.

Measurements

External voltage (busbars), anodes voltage, CVD, current distributions, temperature, heat flux, cell chemistry, cell "starving" and cell MHD "stability" measurements were performed to have a good understanding of the cell status.

Let us summarize the results as follows:

The "Copper insert" cells (average age of 6 months) show a CVD of $268 \pm 9 \text{ mV}$. This is in perfect match with the prediction of 260 mV.

The temperature and electric potential were measured at various locations inside two collector bars. Figure 17 shows the concept.

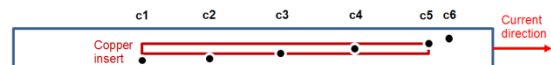


Fig 17: In-situ measurements of temperature and electric potential

The signals were recorded every second for a period of 6 months.

Typical temperature curves are shown in figure 18. Some thermoelements were destroyed after some days, some others stayed alive!

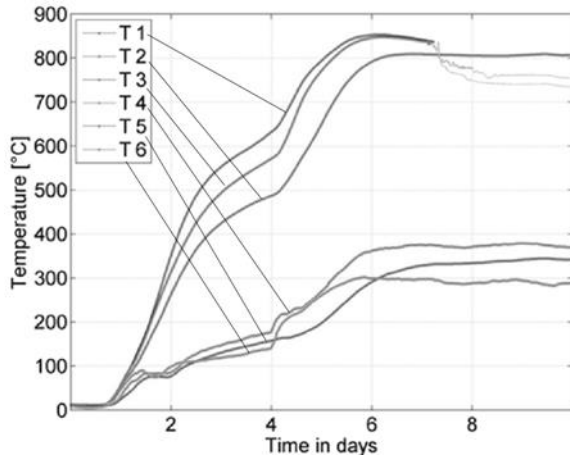


Figure 18: Typical temperature signals for the first days

Important for us was to measure the impact of the copper insert. Figure 19 shows the calculated (curves) and measured (dots) temperature as function of the distance to the bar end. Obviously the predictions fit very well with the measurements and confirm that the copper has a negligible impact on the temperature.

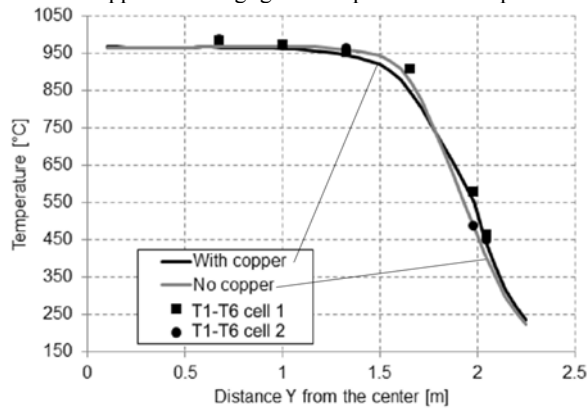


Figure 19: Temperature as function of distance from cell center along collector bars

Figure 20 shows the electric potential as function of the distance from cell center along the collector bars. The red curve is the calculated potential without copper insert. The black curve is the calculated electric potential with the copper insert. The dots are the measurements for two bars using the copper. Here again the agreement is excellent. Interesting is the difference between the two curves telling us that a saving of 60 mV is possible. The CVD measurements have shown a difference of 67.5 mV.

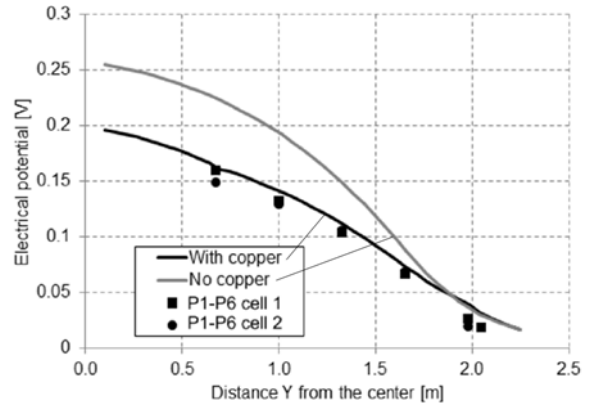


Figure 20: Electrical potential as function of distance from cell center along collector bars

The current density j_x along the copper insert can be calculated from the electric potential measurements using Ohm's law:

$$j_x = -\sigma(T) \frac{\Delta\phi}{\Delta x}$$

Figure 21 shows the calculated current density both for the model (curve) and for the measurements (dots). Here again, the agreement is quite good.

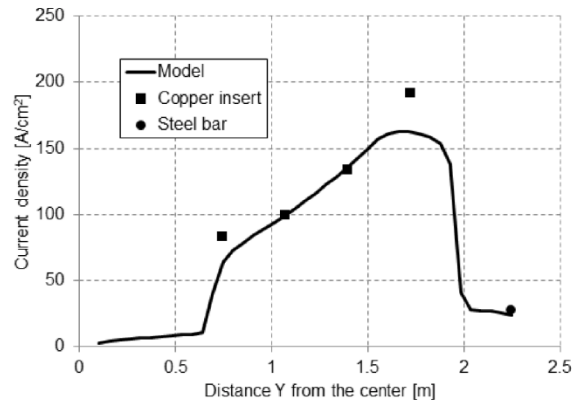


Figure 21: Current density in the middle of the collector bar

We can conclude that the copper insert is doing at least what was expected for the CVD. More important to us, it shows that the current distribution at the cathode surface must be close to what is calculated. Indeed, the model predicts a drastic impact on the cell magneto-hydrodynamic status (velocity field, metal deformation, cell mhd stability). The impact was assessed by decreasing the anode to cathode distance and analysing the cell voltage and a few anode rods currents as function of the ACD decrease.

Figure 22 shows the cell voltage as function of time during the ACD decrease for the Reference cell. The noise level is above 20 mV after 9 mm ACD decrease. Figure 23 shows the same quantity for the "Copper insert" cell. The ACD can be decreased by 15 mm before showing 20 mV noise. A potential of 6 mm ACD decrease is available although the "Copper insert" cell is operated at 24% higher current.

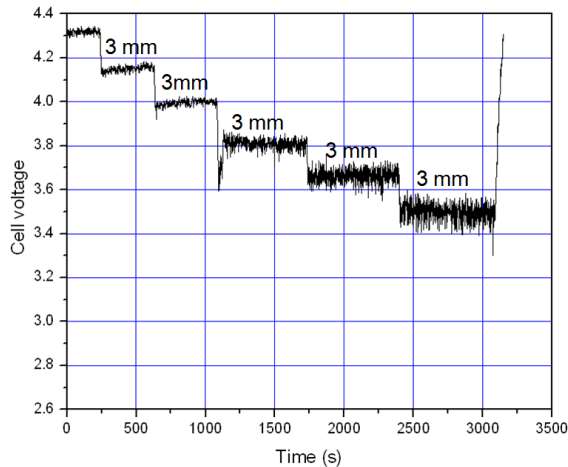


Fig 22: Cell voltage as function of time while decreasing the ACD, Reference cell

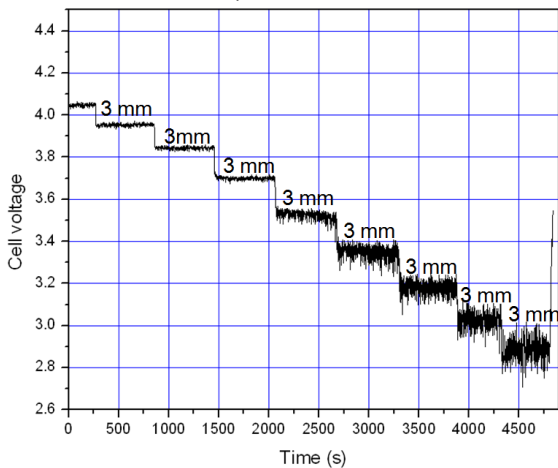


Fig 23: Cell voltage as function of time while decreasing the ACD, “Copper insert” cell

Finally the plant data was analysed. The cell voltage was 4.06 volt (can be noticed in Figure 23) and over the first 6 months the specific energy was lower than 12.9 kWh/kg. The current efficiency must therefore be above 95%. In other words, after 6 months of operation, the “Copper insert” cells show very promising results, in line with the model predictions.

Conclusions

Modeling results and measurements confirm that the use of copper inserts in collector bars may be very beneficial for the cell. Modeling shows that when copper inserts are used correctly, meaning that the heat extraction through the collector bars is in relation with the heat produced and that the current density field in the liquid metal is optimum for the existing busbars system the impact are numerous:

- Lower metal velocity field
- Lower metal deformation
- Lower CVD
- Higher MHD stability
- Potential longer cathode life

This was proven on a set of cells over a period of six months. However, it is important to mention that not only the collector bars must be modified but also the cell lining. Indeed, increasing the heat extraction through the collector bar by using copper in the bar may lead to an unstable cell and even a lower CVD may lead to higher cell voltage. In other words, a perfect match between the energy input, energy output and path for the current in the cell is of prime importance.

Acknowledgement

The authors would like to thank all people involved in this project who helped at collecting the data. In- situ measurement are not easy and a good support from the plant was the key to the success.

References

- [1] R. von Kaenel, J. Antille, Energy savings by using new cathode designs, Proc. 5th International Electrodes Conference, Reykjavik, Iceland, 10-12 May 2011.
- [2] W. Wang Qiang, L. Baokuan, Magneto-hydrodynamic model coupling multiphase flow in aluminum reduction cell with innovative cathode protrusion, Light Metals 2013, 615-619.
- [3] M. Gagnon, P. Goulet, R. Beeler, D. Ziegler, M. Fafard, Optimization of the cathode collector bar with copper insert using finite element method, Light Metals 2013, 621-626.
- [4] M. Blais, M. Désilet, M. Lacroix, Energy savings in aluminum electrolysis cells: effect of cathode design, Light Metals 2013, 627-631.
- [5] Y. Hongjie, L. Fengqin, C. Suwei, Y. Xiaopei, Technology for manufacturing cathodes for aluminum reduction in China, Light Metals 2013, 1239-1243.
- [6] Yan Feiya, M. Dupuis, Z. Jianfei, R. Shaoyong, In depth analysis of energy saving and current efficiency improvement of aluminum reduction cells, Light Metals 2013, 537-542.
- [7] F. Naixiang, P. Jianping, W. Yaowu, D. Yuezhong, L. Xianan, Energy reduction technology for aluminum electrolysis: choice of the cell voltage, Light Metals 2013, 549-552.
- [8] L. Jie, L. Xiao-jun, Z. Hong-liang, L. Ye-xiang, Development of low voltage energy-saving aluminum reduction technology, Light Metals 2013, 557-559.
- [9] F. Naixiang, P. Jianping, W. Yaowu, D. Yuezhong, Y. Jin, Research and application of energy saving technology for aluminum reduction in China, Light Metals 2012, 563-568.